Entropic Elasticity of Single Polymer Chains of Poly(methacrylic acid) Measured by Atomic Force Microscopy

C. Ortiz and G. Hadziioannou*

Department of Polymer Chemistry, University of Groningen, Nijenborgh 4, 9747 AG Groningen, The Netherlands

Received August 6, 1998; Revised Manuscript Received November 30, 1998

ABSTRACT: We have directly measured the entropic elasticity due to the uncoiling of individual polymer chains of poly(methacrylic acid) (PMAA) using the atomic force microscope (AFM). Covalent attachment of one chain end to a substrate and sufficiently low chain grafting densities were achieved by using a mixed monolayer technique that involved the co-chemisorption of (mono)thiol-functionalized PMAA and self-assembling alkanethiols on gold. Single molecule force spectroscopy experiments were carried out in good solvent conditions where the chains were tethered to a Si_3N_4 probe tip via nonspecific physisorption interactions. Upon retraction of the probe tip from the surface, single, continuous, attractive peaks in the force versus distance profiles were frequently observed. These peaks could be fit, for all chain bridging lengths, to entropic-based, statistical mechanical, random-walk formulations, i.e., the *freely jointed chain* (FJC) model and *wormlike chain* (WLC) model. The fits to both models yielded a statistical segment length or persistence length of ≈0.3 nm (approximately the length of a single PMAA monomer unit), thus suggesting that locally the chains are quite flexible. In addition to measuring entropic elasticity, we have also shown that single molecule force spectroscopy experiments are able to provide quantitative information on the statistical nature of adsorption of single polymer chains.

Introduction

Investigations of the mechanical properties of polymers can be approached from three different length scales: macroscopic (millimeters), microscopic (micrometers), and molecular (nanometers). For maximum control and optimization, one must try to understand and interrelate the complex physics occurring at each of these levels. Microscopic and macroscopic deformation of synthetic, random-coil-based, macromolecular systems has been well-studied over the past 60 years and is still one of the most actively investigated research areas. Recently, the inventions of such instruments as the atomic force microscope (AFM),[1] the magnetic levitation force microscope (MLFM),[2] the photonic force microscope (PFM),[3] the surface force apparatus (SFA),[4] micropipet suction (MPS),[5] and optical tweezers (OT)[6] have made it routinely possible to measure the physical properties of materials at the molecular level and led to the new and expanding field of *nanomechanics*.[7] One of the most remarkable achievements in this area has been the direct measurement of the elasticity of single macromolecules.[8−38] Most of the work to date has been conducted on biological polymers such as DNA,[8−16] RNA Polymerase,[17] Dextran,[18] Xanthan,[19] Titin,[20−23] Tenascin,[24] Actin,[25] Kinesin,[26,27] proteoglycans,[28] and human spermatozoa.[29] Research on much smaller synthetic polymers is just beginning.[30−38]

In a typical single molecule force spectroscopy (SMFS) experiment, two segments of a single polymer chain are tethered and stretched apart. The restoring force is measured as a function of the separation distance, thus giving a direct measure of the chain elasticity. At low to moderate extensions, most of the biological polymers studied to date can be described by statistical mechanics models of ideal chains (random walks), such as the inextensible and extensible *freely jointed chain*[40] (FJC) and *wormlikechain*[41] (WLC) models.[8,9,14b,18,20,21a,22,24,28b,35,37] A summary of the force laws corresponding to these models and the materials to which they have been applied is given in Table 1 and will be discussed in more detail in the following sections. By fitting experimental data to these equations, it is possible to separate the entropic and enthalpic components of the deformation and also estimate the statistical segment length, *a* (for the FJC), or the persistence length, *p* (for the WLC).

At large strains (i.e., when the contour length of the molecule is approached or exceeded), many biological polymers undergo significant deviations from these theoretical models due to the intrinsic elasticity of their novel chain architectures. For example, it has been shown that the double-stranded DNA helix exhibits a reversible, conformational transition at a force of ≈0.06 nN to a more tightly coiled, extended structure which is ∼1.7 times its low force contour length.[8,9b,10,12,16] The polysaccharides Dextran[18] and Xanthan[19] also undergo conformational transitions at higher forces (≈0.25 and ≈0.4 nN, respectively) than DNA. Another example of a molecule that displays highly inhomogeneous deformation is the giant muscle protein, Titin, which has a filamentous, modular structure consisting of a linear array of folded immunoglobin (Ig)- and fibronectin (FNIII)-like domains. The force versus distance curve of Titin is characterized by a unique "sawtooth" pattern.[20−23] Each attractive peak has been attributed to stretching of an individual unfolded domain and could be fit to the WLC model. The extracellular matrix protein, Tenascin, which is similar in structure to Titin, also exhibits this unusual sawtooth force profile.[24] Viscoelasticity, hysteresis, stress relaxation, and the effect of environmental conditions such as pH, solvent quality, ionic strength, temperature, etc., are just starting to be examined in such systems. In summary, single molecule force spectroscopy has provided and will continue to provide significant new insights into the fundamental molecular mechanical processes affecting both microscopic and macroscopic behavior.

10.1021/ma981245n CCC: $18.00
Published on Web 01/23/1999

Table 1. Summary of Elasticity Models for Extension of Single Polymer Chains[a]

model	ref	model (fitting) parameters	force laws for extension of single polymer chains	application
freely-jointed chain (FJC)	40a,b	a, n	$F_{chain} = k_BT/aL^*(r/L_{contour})$ low stretches: Gaussian, $F_{chain} = (3k_BT/L_{contour}a)r$ high stretches: $F_{chain} = k_BT/a(1 - r/L_{contour})$	poly(methacrylic acid),[35] poly(dimethylsiloxane)[37]
extensible freely-jointed chain	40c	a, n, $k_{segment}$	$F_{chain} = k_BT/aL^*(r/L_{total})$ $L_{total} = L_{contour} + nF/k_{segment}$	Dextran,[18] ssDNA[9b]
wormlike chain (WLC)	41a,b	p, n	$F_{chain} = (k_BT/p)(^1/_4(1 - r/L_{contour})^{-2} - ^1/_4 + r/L_{contour})$ low stretches: Gaussian high stretches: $F_{chain} = k_BT/4p(1 - r/L_{contour})^2$	Titin,[20,21a,22] Tenascin,[24] Proteoglycans, [28b] poly(dimethylsiloxane)[37]
extensible wormlike chain	41c	p, n, $k_{segment}$	$F_{chain} = (k_BT/p)(^1/_4(1 - r/L_{total})^{-2} - ^1/_4 + r/L_{total})$ high stretches: $r = L_{contour}(1 - 0.5(k_BT/F_{chain}/k_{segment})$	dsDNA[8,9,14b]

[a] F_{chain} (nN) is the elastic, restoring force of the polymer chain, r (nm) is the chain end-to-end separation distance, k_B (J/K) is the Boltzmann constant (=1.38106 × 10^{-23}), T (K) is the absolute temperature (298), a (nm) is the statistical segment length (FJC), p (nm) is the persistence length (WLC), $L(X)$ is the Langevin function (= coth $X - 1/X$, $X = Fa/k_BT$), L^* is the inverse Langevin function, $L_{contour}$ (nm) is the fully, extended contour length of the chain = na (FJC) or np (WLC), n is the number of chain segments, L_{total} (nm) is the fully extended length of the chain including extensibility of the chain segments, and $k_{segment}$ (N/m) is the segmental spring constant.

In this paper, we present the results of SMFS experiments carried out with the AFM on the synthetic polyelectrolyte, poly(methacrylic acid) (PMAA). The chains have a fully extended contour length of ≈120 nm and, hence, are much smaller than most of the biopolymers studied to date. A mixed monolayer technique[42] was employed to reduce the chain grafting density and covalently attach one chain end to a substrate. A Si_3N_4 probe tip was used to pick up the chains via nonspecific physisorption interactions. Monofunctional chains eliminated the possibility of covalently bound loops, as well as chain segments bound to the tip after numerous experiments. Upon retraction of the probe tip from the surface, we observed individual, continuous, attractive peaks in the force versus distance profiles. By fitting the data to theoretical models, it became evident that the measured force corresponded to the elastic, entropic, restoring force due to uncoiling of individual polymer chains. Our subsequent analysis included the calculation of the statistical segment and persistence lengths, the extended length of the adsorbed bridging chain segment, and the adsorption force tethering the chain to the probe tip.

Experimental Section

Materials. 11-Mercapto-1-dodecanol (HS-$[CH_2]_{11}$-OH) was purchased from Aldrich Chemical Co. (97% pure) and used as received. Monofunctional thiol-terminated poly(methacrylic acid) (PMAA-SH) was synthesized via a photoiniferter technique.[43] The weight-average molecular weight, M_w, was found to be ≈66 200 g/mol and the polydispersity, M_w/M_n, to be ≈2 (where M_n is the number-average molecular weight) by gel permeation chromatography (GPC) and light scattering (Dawn DSP-F, wavelength = 632.8 nm). The average contour length of the chain, $L_{contour} = nl$ (for a freely jointed chain where n is the number of C−C backbone bonds and is equal to $2N$, N is the degree of polymerization and equal to M_n/monomer formula weight, and l is the length of a C−C backbone bond ≈ 0.154 nm), was calculated to be ≈120 nm. The radius of gyration of neutral, isolated PMAA chains of this molecular weight in solution, $R_g = \sigma\sqrt{C_\infty}\sqrt{nl})/\sqrt{6}$ (where C_∞ is the characteristic ratio ≈ 10 and σ is the steric parameter ≈ 2), was calculated to be 10 nm. The actual value should be somewhat greater than R_g since it is believed that at pH = 7 the PMAA chains are partially ionized due to dissociation of a fraction of the carboxylic acid groups.[44]

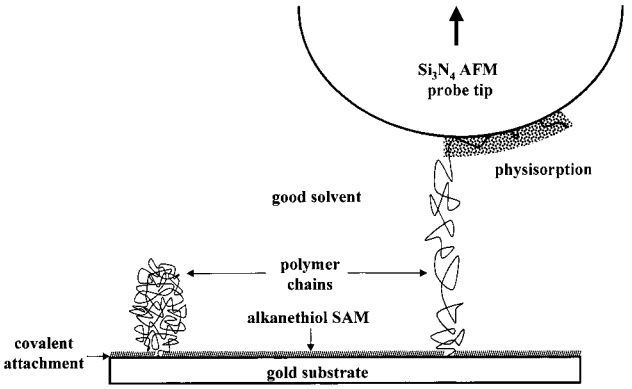

Figure 1. Schematic of AFM experiment on mixed monolayer of poly(methacrylic acid) and alkanethiol SAM.

Gold Evaporation. Atomically flat, polycrystalline gold substrates were prepared by thermal evaporation according to methods described in the literature.[45] Approximately 10 cm × 10 cm of clear, ruby, muscovite mica, grade 2 (Mica New York Corp.) was cleaved in air and immediately placed in a vacuum chamber of a diffusion-pumped thermal evaporator (Edwards Auto 306). The mica sheet was heated to 400 °C using a hot stage and allowed to equilibriate for a few hours under vacuum. A 30 nm sample of gold (99.99% pure, 0.5 mm diameter gold wire, Schöne Edelmetalen) was evaporated at a rate of ≈0.1 nm/s and at a pressure of ≈10^{-7} Mbar. The thickness was monitored with a quartz crystal oscillator (Intellemetrics, Ltd., PE 108-02, 6 MHz). The plate was annealed for an additional 2−3 h at 400 °C, after which time the heat was turned off and allowed to cool slowly overnight under vacuum.

Sample Preparation. Mixed monolayers were prepared according to methods described in the literature[42] as shown in Figure 1. Gold substrates were exposed to a two-component solution of the HS-PMAA and the 11-mercapto-1-dodecanol in DEMI water (a good solvent for the PMAA and a bad solvent for the alkanethiol) for 24 h. *n*-Alkanethiol compounds on Au (111) surfaces are well-known to spontaneously form a chemically and mechanically stable, highly ordered, crystalline-like self-assembling monolayer in which the molecules are covalently attached to the surface via a gold−thiolate bond and tilted at ≈30° from the substrate normal.[46] The ratio of the number of moles of the PMAA-SH (n_{PMAA}) to the total number of moles of the two components ($n_{PMAA} + n_{11-mercapto-1-dodecanol}$) in the solution was $\chi_{PMAA} \approx 0.85$, and the polymer concentration was $c_{PMAA} \approx 1$ mg/mL. After 24 h the substrates were removed from the solution and rinsed exhaustively with DEMI water. These adsorption conditions are known to produce isolated, well-separated polymer chains with a distance between neighboring chains, $D \approx 100-200$ nm.[42] Flexible, neutral chains should exhibit a "mushroom"-like conformation for $D > 2R_g$ with the polymer height from the surface, $L_0 \approx$

R_g.[47] Once again, if there are a significant number of carboxylic acid groups dissociated, electrostatic repulsion along the chain will cause extension away from the surface, i.e., $L_0 > R_g$.

Atomic Force Microscopy: Force Spectroscopy. Force spectroscopy experiments were performed with the Topometrix Explorer (TMX1010) AFM in DEMI water. The experimental setup employs an open liquid cell design with the cantilever mounted underneath a Teflon-coated piezoelectric tube scanner (E299701, 0.9 μm z-range). Commercially available V-shaped Si_3N_4 cantilevers with the following dimensions were used: outer leg length $\approx$ 200 μm, inner leg length $\approx$ 150 μm, leg width $\approx$ 18 μm, leg thickness $\approx$ 0.6 μm. The resonant frequency of the cantilever was reported to be $\approx$18 kHz and the spring constant, $k_c \approx 0.032$ N/m. The pyramidal probe tip had a height $\approx$ 1 μm, width $\approx$ 4 μm, and a radius of curvature of $\approx$20$-$50 nm. The backside of the cantilevers were coated with a layer of gold by the manufacturer (thickness $\approx$30 nm) to increase reflectivity.

In a typical force versus distance measurement, the probe tip is first brought out of feedback and raised to $\approx$1000 nm above the sample surface. Data acquisition is initiated, and the sensor output difference of the two horizontal quadrants of a four-quadrant position-sensitive photodetector, s (nA), is recorded as a function of z-piezo deflection, z (nm), where z is the direction normal to the substrate. The piezo incrementally moves the tip toward the sample in the z-direction relative to the fixed sample position. The z-piezo deflection rate, dz/dt, was 0.25 μm/s. When contact is made, the tip continues to compress into the surface until a repulsive force of several nanonewtons is achieved. The piezo then reverses direction, and the cantilever is retracted away from the sample. All data presented are for a single approach and decompression per polymer chain.

The raw data were exported as ASCII files and imported into a spreadsheet analysis program. The sensor output, s, was converted into the cantilever deflection, δ_c (nm), by assuming that the change in z-piezo deflection, dz, was equivalent to the change in cantilever deflection, $d\delta_c$, in the repulsive, contact regime of constant compliance (reasonably accurate for stiff samples):

$$\delta_c = s/m \tag{1}$$

where m (nA/nm) is the slope of sensor output versus z-piezo deflection curve in the constant compliance regime or "piezo senstivity". The force was then calculated by using Hooke's law for a linear elastic spring:

$$F = k_c\delta_c \tag{2}$$

where F (nN) is the force exerted by the sample on the cantilever (which is equivalent to the force exerted by the cantilever on sample) and k_c (nN/nm) is the cantilever spring constant. k_c was determined for each individual cantilever according to a nondestructive method described in the literature.[48] The point of zero force corresponding to the undeflected cantilever was obtained from data taken at large probe$-$tip separations. The usual convention of (+) for repulsive forces and (−) for attractive forces was employed. The error in AFM force measurements is due to calculation of the piezo sensitivity ($\pm$5%), the spring constant calibration ($\pm$10%), and nonlinearities of the photodetector associated with the finite size of the laser spot ($\pm$2%). The limiting force resolution is ultimately the experimental background noise, which was approximately $\pm$0.02 nN.

The z-piezo deflection, z, was converted into the tip$-$sample separation distance (henceforth referred to as "distance"), d, by correcting for the cantilever displacement due to the applied force:

$$d = z - \delta_c \tag{3}$$

where δ_c is calculated from eq 2. The point of zero distance was approximated as the point where the tip meets the stiff substrate and the force versus distance curve becomes nearly vertical (the region of constant compliance). The error in the z-piezo deflection measurements ($\pm$10%) is primarily due to time-dependent nonlinearities in the piezoelectric scanner (e.g., aging, creep, etc.).

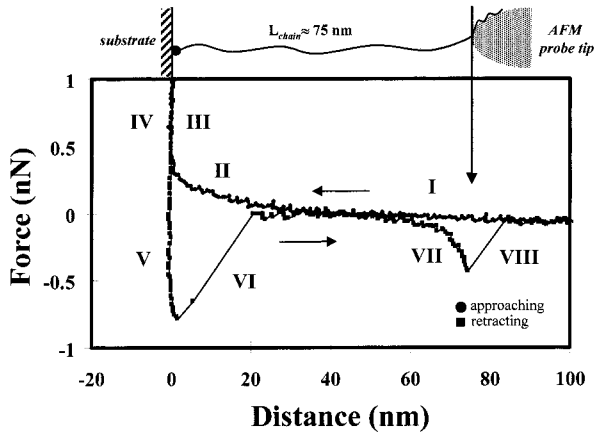

Figure 2. (a) Typical force versus distance curve for mixed monolayer of poly(methacrylic acid) and alkanethiol SAM: I, no tip$-$sample interaction; II, compression of single polymer chain; III/IV, repulsive contact with substrate; V, attractive peak due to surface adhesion; VI, cantilever "pulls off" surface; VII, attractive peak due to stretching of a single polymer chain; VIII, polymer chain desorbs suddenly from probe tip.

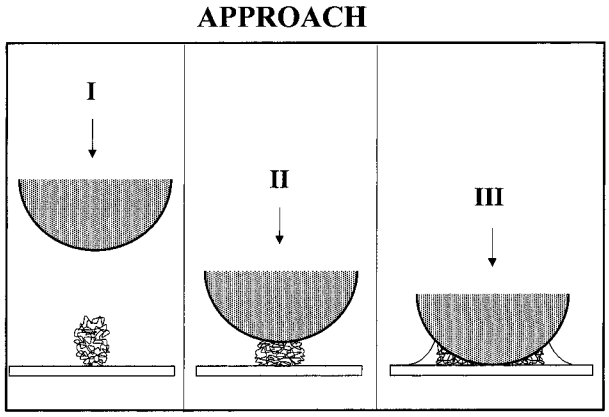

Figure 3. Schematics of different regions of force curve on approach labeled in Figure 2 (*alkanethiol SAM is not shown): I, no tip$-$sample interaction; II, compression of single polymer chain/chain segments begin to adsorb to probe tip; III, repulsive contact with substrate.

Results and Discussion

Figure 2 is an example of a typical force versus distance curve observed in the AFM experiments conducted on the mixed monolayer of HS-PMAA and HS-$[CH_2]_{11}$-OH.

Force Profile on Approach. Figure 3 shows schematically the processes occurring on approach in each of the regions corresponding to those labeled in Figure 2. Far away from the surface (I), the force is zero and there is no interaction between the tip and sample. As the cantilever approaches the surface, a nonlinear repulsive force is observed to begin at $d \approx 50$ nm ($\approx 5R_g$), corresponding to the compression of a single polymer chain (II). Since this interaction range is larger than R_g (expected for neutral polymer "mushrooms"), the chains are thought to be somewhat extended away from the surface.

The large, nonlinear repulsive force ($F_{approach}(max) \approx$ 0.35 nN) measured on approach is difficult to model

theoretically because there are a number of different phenomena occurring simultaneously which make both repulsive and attractive contributions to the net force. These processes may include one or more of the following: (1) the electrostatic repulsion between the negatively charged Si_3N_4 tip which contains a fraction of ionized silanol (SiO^-) and silylamine (SiN^-) groups[49] and the negatively charged PMAA chain ($-COO^-$),[44] (2) the repulsive, entropic elastic force due to stretching of the polymer chain in the *x*/*y* plane perpendicular to the compression axis[50] (discussed in detail later on), (3) the electrostatic repulsion between negatively charged $-COO^-$ groups along the polymer chain, (4) the repulsive polymer chain confinement penalty between the two surfaces (tip and substrate) during compression,[50] (5) tip−surface (polymer and SAM) hydrophilic−hydrophilic hydration repulsion,[51] (6) the attractive entropic, elastic force due to stretching of the chain in the *z*-direction during chain segment adsorption to probe tip, and (7) the tip−SAM attractive interaction due to van der Waals and hydrogen bonding between silylamine ($SiNH_2$, SiNH) and silanol (SiOH) groups on the probe tip[49] and the hydroxyl (−OH) groups of the SAM. Similar experiments[35] done on the same system with a gold-coated AFM tip (which is hydrophobic and neutral) also show a large, nonlinear repulsive force of approximately the same magnitude observed here, suggesting that the tip−polymer electrostatic and hydrophilic interactions are minimal. This indicates that there is a significant contribution to the compressive repulsive force by the electrostatic repulsion between negatively charged $-COO^-$ groups along the polymer chain, which are becoming increasingly confined and compressed as the experiment proceeds.

Even if we neglect electrostatic, confinement, adsorption, van der Waals, and H-bonding effects, the force law equations given in Table 1 for extension of the FJC and WLC cannot be used directly to describe the repulsive, entropic, elastic force due to compression of a single polymer chain. This is because the chain extension in the *x*/*y* plane is nonuniform (varies with distance from the tip apex) and depends on the radius of curvature of the tip relative to the radius of gyration of the chain, the shape of the probe tip, and the alignment of the tip relative to the attachment point. Scaling law approaches have recently been taken to in order explore this problem.[50]

In many cases, the large repulsive force due to the presence of the polymer chain screens out a typical discontinuous "jump-to-contact", and instead, the probe tip makes contact with the gold substrate smoothly, leading to a rapidly increasing force (III).

Force Profile on Retraction. Figure 4 shows schematically the processes occurring on retraction in each of the regions corresponding to those labeled in Figure 2. Decompression of the gold (IV) is reversible (elastic) and follows the same force versus distance path as on compression. With continued retraction, the probe tip exhibits adhesion to the surface characterized by hysteresis in the force versus distance curve and an attractive force which decreases rapidly and linearly with distance (V). This adhesion ($F_{\text{adhesion}} \approx 0.75$ nN) is attributed primarily to van der Waals and hydrogen-bonding interactions between the tip and SAM.

As the piezo continues to retract, the cantilever force eventually becomes equivalent to the adhesion force and $\partial F/\partial z = k_c$. Immediately after, the cantilever exhibits a

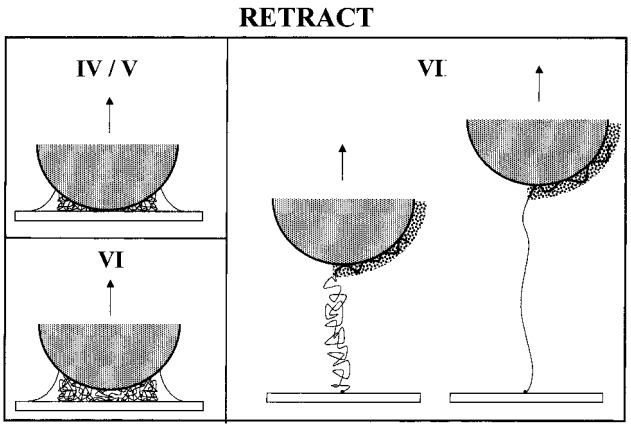

Figure 4. Schematics of different regions of force curve on retraction labeled in Figure 2 (alkanethiol SAM is not shown): IV, repulsive contact with substrate; V, contact with substrate maintained due to surface adhesion; VI, cantilever "pulls off" surface; VII, bridging chain segment stretches.

mechanical instability and suddenly "pulls off" the surface (VI). After a short distance, the force does not stabilize at exactly zero but returns to a small (+) value consistent with the repulsive, compressive force on approach. From our data, it is difficult to conclusively show the absence of hysteresis in the polymer chain decompression due to the significant amount of surface adhesion. However, other experiments[35] done on the same system with a gold-coated AFM tip (which eliminates H-bonding and minimizes the surface adhesion) show complete reversibility of the compression, indicating minimal interaction between the polymer and SAM. This is in contrast to pure, adsorbing polymer layers which exhibit large, nonequilibrium relaxation effects and marked hysteresis, possibly due to additional monomers being adsorbed onto the surfaces under compression.[52]

As the experiment proceeds, a single attractive peak is observed[53] in which the force increases nonlinearly with distance (VII). This attractive peak is attributed to the stretching of an *individual* polymer chain which had become physically adsorbed to the tip on approach and bridges the substrate and tip. The tethering of single polymer chains is facilitated by the low surface grafting density, as well as the small probe tip radius. In fact, it has been shown that picking up single polymer chains via physisorption forces is probable even in pure polymer layers.[20−24]

For linear macromolecules, physisorption takes place through the formation of trains (a series of consecutively adsorbed segments), loops (segments terminally bound but only in contact with solvent), and tails (one end bound and the other dangling in solution).[54] The percentage of each type of linkage depends on a number of factors such as solvent quality, temperature, polymer−tip contact area, time, force, polymer segment−tip interaction energy, number of available adsorption sites, chain stiffness, etc. The adsorption of PMAA chain segments to the Si_3N_4 probe tip will be a balance between the tip ($-SiO^-$, $-SiN^-$)−polymer ($-COO^-$) electrostatic repulsion, tip−polymer hydrophilic repulsion, attractive van der Waals forces, and hydrogen bonding between the tip (−OH, −NH, $-NH_2$) and the polymer chain (−COOH, $-COO^-$). Hence, the chain conformation on the surface (loops, trains, tails) is unknown.

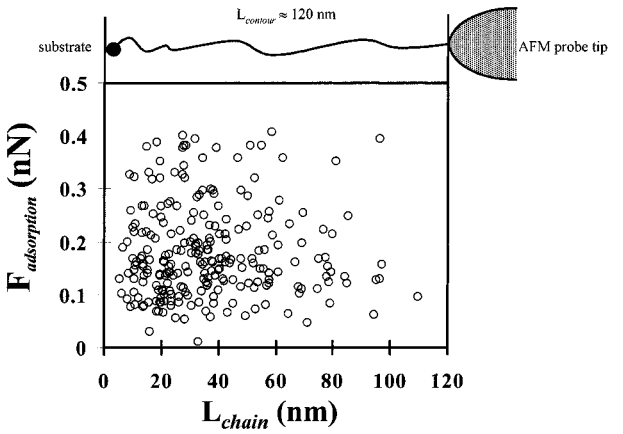

Figure 5. Adsorption force versus adsorbed polymer chain segment length for AFM force versus distance curves on single poly(methacrylic acid) chains compared to $L_{contour}$, the average chain contour length calculated from average polymer molecular weight.

At high enough extensions, the elastic restoring force of the chain becomes equal to and just exceeds the adsorption force tethering the chain segments to the tip. At this point (VIII), the tethered chain segments suddenly desorb from the tip, and the cantilever is returned back to its undeflected position corresponding to zero force.

Peak Analysis. Two values were recorded for each attractive peak in the numerous force versus distance curves taken (excluding the adhesion peaks): the attractive peak minimum which is equivalent to the adsorption force, $F_{adsorption,}$ and the extended length of the adsorbed polymer chain segment, L_{chain}, which is equivalent to the distance at the attractive peak minimum. Figure 5 plots the values of $F_{adsorption}$ versus L_{chain} where each data point corresponds to a single attractive peak. Figure 6 gives the probability distribution histograms, P, calculated from these data (where P is the number of data points within a given interval/total number of data points).

$F_{adsorption}$ is found to be <0.5 nN with a mean value of 0.19 ± 0.11 nN, which confirms that the chain tethering mechanism is indeed physisorption.[20−24,54] The distribution of $F_{adsorption}$ is thought to result from variations in the number of chain segments adsorbed to the tip. Since $F_{adsorption}$ is much less than the predicted force necessary to cleave the weakest covalent bond (i.e., the Au−S bond; $F_{cleavage} \approx 2-3$ nN[55,56]), it is assured that each polymer chain always detaches from the tip after each experiment.

L_{chain} is found to be <110 nm with a mean value of 36.9 ± 21.6 nm, which is consistent with the length of the fully extended coil, $L_{contour} \approx 120$ nm, calculated for a freely jointed chain from the number-average molecular weight. The wide variation of L_{chain} is due to the fact that the tip can adsorb at sites along the entire length of the chain (i.e., it is a nonspecific interaction), as well as the high polydispersity of the chains.

Comparison with Entropic-Based Statistical Mechanics Models (Table 1). The most general theoretical formulation is the *freely jointed chain* (FJC) model[40a,b] which considers a single, isolated, flexible, polymer chain without any long-range interactions (Figure 7a). It is a statistical mechanical, random walk formulation of a hypothetical polymer chain consisting of n rigid segments of length, a, joined in linear succession and

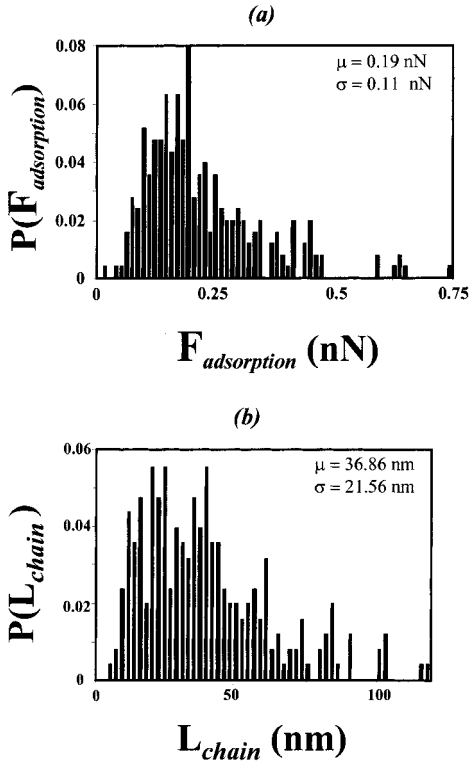

Figure 6. Probability distributions for (a) adsorption force and (b) adsorbed polymer chain length for AFM force versus distance curves on single poly(methacrylic acid) chains; μ = mean, σ = standard deviation.

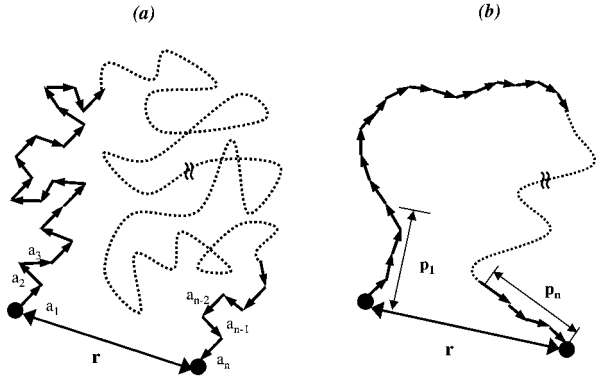

Figure 7. Schematics of the (a) *freely jointed chain* model[40] and (b) *wormlike chain* model.[41]

connected by freely rotating pivots. a is the statistical or Kuhn segment length and represents the distance over which the polymer chain is directionally correlated (i.e., a is a measure of the local chain stiffness or resistance to bending). The *wormlike chain* (WLC) model[41a,b] (Figure 7b) describes a polymer chain that is intermediate between a rigid-rod and a flexible coil and takes into account both local stiffness (described by the persistence length, p) and long-range flexibility. The distinguishing property of the WLC is that the chain is treated as an isotropic, homogeneous rod whose trajectory varies continuously and smoothly through space, as opposed to the jagged contours of the more flexible FJC.

Upon stretching a FJC or WLC, each statistical chain segment continuously rotates itself to reorient along the applied stress direction. The elastic restoring force, F_{chain}, originates from a reduction in the number of possible chain configurations and, hence, a reduction in

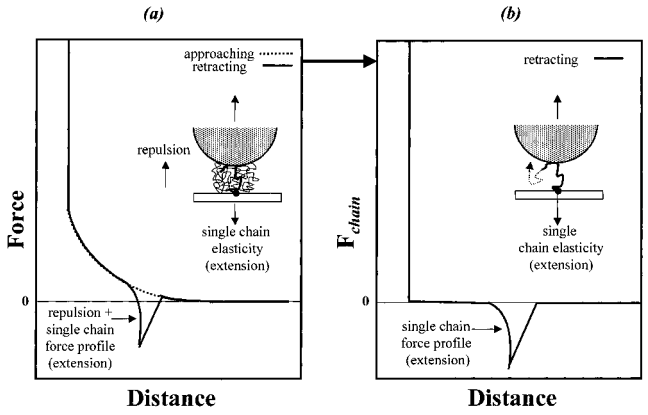

Figure 8. Calculation of the force profile for the extension of a single polymer chain (shown schematically): (a) measured force versus distance profile and (b) force versus distance profile of a single polymer chain after repulsion correction (eq 4).

the configurational entropy. Both models have been modified in order to take into account enthalpic deformation or "extensibility" of the chain segments by introducing a segmental spring constant, $k_{segment}$.[40c,41c] The force law equations and fitting parameters for all of these models are given in Table 1.

To accurately compare our experimental data (i.e., the attractive peaks observed on retraction) with theoretical models and the equations given in Table 1, a "correction" was made to the experimental data as shown schematically in Figure 8. Here we subtract the nonlinear, repulsive force observed on approach, $F_{approach}$[57] (which also occurs and is approximately equal to that on retraction[35]) from the measured retraction force, $F_{retract}$, to yield solely the entropic, elastic force due to stretching the polymer chain in the z-direction, F_{chain}:

$$F_{chain} = F_{retract} - F_{approach} \quad (4)$$

This correction becomes significant for $L_{chain} < L_0 \approx 50$ nm.

Figure 9a shows the experimental data (from eq 4) for the extension of single polymer chains on retraction (i.e., numerous force versus distance experiments where each peak corresponds to a single experiment) fit to the FJC model (equation given in Table 1). Since for each experiment the length of the bridging chain segment is variable and unknown (due to the nonspecific physisorption tethering mechanism and chain polydispersity), we have two fitting parameters: the statistical segment length, a, and the number of statistical chain segments, n. n was adjusted to best fit the data for each curve, and a was found to be 0.33 ± 0.05 nm. Here it is seen that the data could be fit very well to the FJC model for all bridging chain lengths using the same value of a (and only this value of a). This result was reproduced several hundred times, using different samples and at different locations of the same sample. If the distance data (x-axis) in Figure 9a is normalized by the value of $L_{(contour)s}$ ($=na$) obtained from each theoretical fit (Figure 9b), a "master curve" can be produced which superimposes all of the data onto a single plot. Here we see that data are obtained starting at $\approx 0.4L_{contour}$, and the final extended length of the bridging chain segment, L_{chain}, is $\approx 0.98L_{(contour)s}$.

Figure 10a,b shows that the same experimental data could also be fit to the WLC model (equation given in

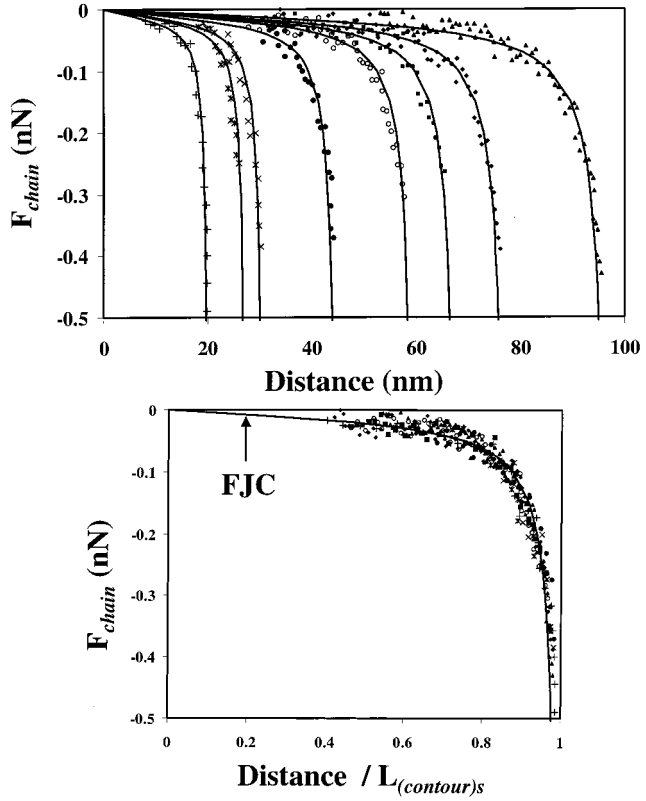

Figure 9. (a, top) Experimental data of numerous force versus distance experiments (each peak corresponds to a single experiment) for single chains of poly(methacrylic acid) fit to the freely jointed chain model ($a = 0.33$ nm, $n = 61$, 83, 93, 136, 181, 206, 235, 295). (b, bottom) Master curve of experimental data for stretching single chains of poly(methacrylic acid) compared to freely jointed chain model.

Table 1) using a persistence length, p, of 0.28 ± 0.05 nm. The fact that we have two fitting parameters allows us to fit the data equally well to both models. The final extended length of the bridging chain segment, L_{chain}, was found to be $\approx 0.92L_{(contour)s}$ for the WLC.

As seen in Figures 9 and 10, the theoretical models predict a linear force versus distance curve at low extensions, where the chain behaves like an entropic, Hookean spring. At moderate strains, a nonlinear, non-Gaussian force versus distance curve is observed. At high stretches, the force rapidly diverges as the contour length is approached because the chain has fewer and fewer configurational options and, hence, less entropy. Theoretically, when the distance becomes equal to the contour length of the bridging chain segment, $L_{(contour)s}$, the chain becomes a straight line, and there is only one configuration available corresponding to zero entropy. No additional extensibility of the segments was needed to fit the data, and the deformation can be assumed to be purely entropic.[58]

Conclusions

In summary, we have directly measured the force versus separation profiles of individual polymer chains of the synthetic polyelectrolyte, poly(methacrylic acid), as they are extended between a substrate and an AFM probe tip. The reproducibility of the results, as well as the correlation between peak distances and $L_{contour}$, confirms that primarily single chains were stretched. By comparing our data with the inextensible FJC and WLC models, we established the nature of the deforma-

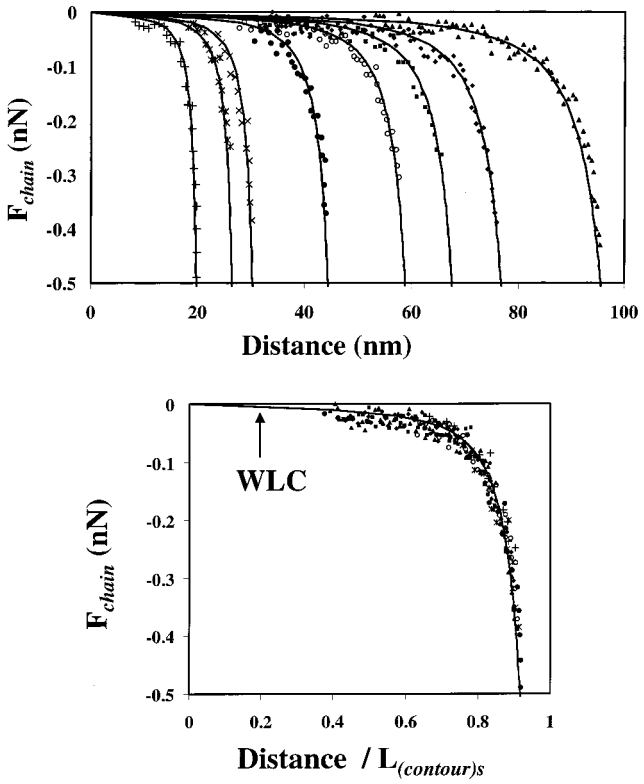

Figure 10. (a, top) Experimental data of numerous force versus distance experiments (each peak corresponds to a single experiment) for single chains of poly(methacrylic acid) fit to the wormlike chain model ($p = 0.28$ nm, $n = 77$, 103, 118, 173, 229, 263, 299, 372). (b, bottom) Master curve of experimental data for stretching single chains of poly(methacrylic acid) compared to wormlike chain model.

tion as solely entropic and estimated the statistical segment and persistence lengths (≈0.3 nm). In addition to probing mechanical properties at the nanometer scale, we have shown that single molecule force spectroscopy can also provide quantitative information on the statistical nature of adsorption.

Acknowledgment. The authors acknowledge Dr. Vasileios Koutsos and Dr. Lionel Garnier, who conducted many preliminary experiments for this work as well as first observed the single chain elasticity profiles in the PMAA system.[35] The authors also thank Eric van der Vegte for synthesis of the PMAA, Ilya Reviakine for help with programming of the statistical analysis software, and Eugene Terentjev and Carlos Marques for helpful discussions. This research was sponsored by a National Science Foundation (NSF)/NATO postdoctoral fellowship.

References and Notes

(1) Binnig, G.; Quate, C. F.; Gerber, Ch. *Phys. Rev. Lett.* **1986**, *56* (9), 930−933.
(2) (a) Gauthier-Manuel, B.; Garnier, L. *Rev. Sci. Instrum.* **1997**, *68* (6), 2486−2489. (b) Gauthier-Manuel, B. *Europhys. Lett.* **1992**, *17*, 195−200.
(3) Florin, E.-L.; Pralle, A.; Hoerber, J. K. H.; Stelzer, E. H. K. *J. Struct. Biol.* **1997**, *119* (2), 202−211.
(4) Israelachvili, J. N.; Adams, G. E. *J. Chem. Soc., Faraday Trans. 1* **1978**, *74*, 975.
(5) Evans, E.; Ritchie, K.; Merkel, R. *Biophys. J.* **1995**, *68*, 2580−2587.
(6) (a) Ashkin, A.; Dziedzic, J. M. *Phys. Rev. Lett.* **1985**, *54*, 1245−1248. (b) Ashkin, A.; Dziedzic, J. M.; Bjorkholm, J. E.; Chu, S. *Opt. Lett.* **1986**, *11*, 288−290.
(7) See for example: Burnham, N. A.; Colton, R. J. In *Scanning Tunneling Microscopy and Spectroscopy: Theory, Techniques, and Applications*; Bonnel, D. A., Ed.; VCH Publishers: New York, 1993; pp 191−249.
(8) Austin, R. H.; Brody, J. P.; Cox, E. C.; Duke, T.; Volkmuth, W. *Phys. Today* **1997**, *50*, 32−38.
(9) (a) Smith, S. B.; Finzi, L.; Bustamante, C. *Science* **1992**, *258*, 1122−1126. (b) Smith, S. B.; Cui, Y.; Bustamante, C. *Science* **1996**, *271*, 795−799. (c) Bustamante, C.; Marko, J. F.; Siggia, E. D.; Smith, S. B. *Science* **1994**, *265*, 1599−1600. (d) Baumann, C. G.; Smith, S. B.; Bloomfield, V. A.; Bustamante, C. *PNAS* **1997**, *94*, 6185−6190.
(10) Cluzel, P.; LeBrun, A.; Heller, C.; Lavery, R.; Viovy, J.-L.; Chatenay, D.; Caron, F. *Science* **1996**, *271*, 792−794.
(11) Perkins, T. T.; Smith, D. E.; Larson, R. G.; Chu, S. *Science* **1995**, *268*, 83−87.
(12) Shivashankar, G. V.; Libchaber, A. *Appl. Phys. Lett.* **1997**, *71* (25), 3727−3729.
(13) (a) Bensimon, D.; Simon, A. J.; Croquette, V.; Bensimon, A. *Phys. Rev. Lett.* **1995**, *74* (23), 4754−4757. (b) Strick, T. R.; Allemand, J.-F.; Besimon, D.; Bensimon, A.; Croquette, V. *Science* **1996**, *271*, 1835−1837.
(14) (a) Yin, H.; Wang, M. D.; Svoboda, K.; Landick, R.; Block, S. M.; Gelles, J. *Science* **1995**, *270*, 1653−1656. (b) Wang, M. D.; Yin, H.; Landick, R.; Gelles, J.; Block, S. M. *Biophys. J.* **1997**, *72*, 1335−1346.
(15) Lee, G. U.; Chrisey, L. A.; Colton, R. J. *Science* **1994**, *266*, 771−773.
(16) Noy, A.; Vezenov, D. V.; Kayyem, J. F.; Meade, T. J.; Lieber, C. M. *Chem. Biol.* **1997**, *4*, 519−527.
(17) Wang, M. D.; Schnitzer, M. J.; Yin, H.; Landick, R.; Gelles, J.; Block, S. M. *Science* **1998**, *282*, 902.
(18) Rief, M.; Oesterhelt, F.; Heymann, B.; Gaub, H. E. *Science* **1997**, *275*, 1295−1297.
(19) Li, H.; Rief, M.; Oesterhelt, F.; Gaub, H. E. *Adv. Mater.* **1998**, *3* (4), 316−319.
(20) Rief, M.; Gautel, M.; Oesterhelt, F.; Fernandez, J. M.; Gaub, H. E. *Science* **1997**, *276*, 1109−1112.
(21) (a) Kellermayer, M. S. Z.; Smith, S. B.; Granzier, H. L.; Bustamente, C. *Science* **1997**, *276*, 1112−1116. (b) Kellermayer, M. S. Z.; Granzier, H. L. *Biochem. Biophys. Res. Commun.* **1996**, *221*, 491−497.
(22) Tskhovrebova, L.; Trinick, J.; Sleep, J. A.; Simmons, R. M. *Nature* **1997**, *387*, 308−312.
(23) Erickson, H. P. *Science* **1997**, *276*, 1090−1092.
(24) Oberhauser, A. F.; Marszalek, P. E.; Erickson, H. P.; Fernandez, J. M. *Nature* **1998**, *393*, 181.
(25) Kishyno, A.; Yanagida, T. *Nature* **1988**, *334*, 74−76.
(26) (a) Svoboda, K.; Schmidt, C. F.; Schnapp, B. J.; Block, S. M. *Nature* **1993**, *365*, 721−727. (b) Svoboda, K.; Block, S. M. *Cell* **1994**, *77* (5), 773−784.
(27) (a) Kuo, S. C.; Sheetz, M. P. *Science* **1993**, *260*, 232−234. (b) Kuo, S. C.; Ramanathan, K.; Sorg, B. *Biophys. J.* **1995**, *68* (4), *74* (1).
(28) (a) Dammer, U.; Popescu, O.; Wagner, P.; Anselmetti, D.; Güntherodt, H.-J.; Misevic, G. N. *Science* **1995**, *267*, 1173−1175. (b) Fritz, J.; Anselmetti, D.; Jarchow, J.; Fernàndez-Busquets, X. *J. Struct. Biol.* **1997**, *119*, 165−171.
(29) (a) König, K.; Svaasand, L.; Yagang, L.; Sonek, G.; Patrizio, P.; Tadir, Y.; Berns, M. W.; Tromberg, B. J. *Cell. Mol. Biol.* **1996**, *42* (4), 501−509.
(30) Kikuchi, H.; Yokoyama, N.; Kajiyama, T. *Chem. Lett.* **1997**, *11*, 1107−1108.
(31) Jensenius, H.; Zocchi, G. *Phys. Rev. Lett.* **1997**, *79* (25), 5030−5033.
(32) Kamiti, M.; van de Ven, T. G. M. *Macromolecules* **1996**, *29*, 1191−1194.
(33) Volpert, E.; Selb, J.; Candau, F.; Green, N.; Argillier, J. F.; Audibert, A. *Langmuir* **1998**, *14*, 1870−1879.
(34) Lea, A. S.; Andrade, J. D.; Hlady, V. In *Colloid and Polymer Interactions: Particulate, Amphiphilic, and Biological Surface*; ACS Symposium Series; Dublin, P. L., Tong, P., Eds.; American Chemical Society: Washington, DC, 1993; Chapter 20, pp 266−279.
(35) Koutsos, V. Ph.D. Thesis, University of Groningen, 1997.
(36) Courvoisier, A.; Isel, F.; François, J.; Maaloum, M. *Langmuir* **1998**, *14*, 3727−3729.
(37) Sendon, T. J.; di Meglio, J.-M.; Auroy, P. *Eur. Phys. J. B.* **1998**, *36* (3), 211−216.
(38) Hinderdorfer, P.; Baumgartner, W.; Gruber, H. J.; Schilcher, K.; Schindler, H. *PNAS* **1996**, *93*, 3477−3481.
(39) Deleted in proof.

(40) (a) Kuhn, W. *Kolloid Z.* **1934**, *68*, 2. (b) Guth, E.; Mark, H. *Monatsh. Chem.* **1934**, *65*, 93. (c) Marko, J. F.; Siggia, E. D. *Macromolecules* **1995**, *28*, 8759−8770.
(41) (a) Kratky, O.; Porod, G. *Recl. Trav. Chim. Pas-Bas* **1949**, *68*, 1106. (b) Fixmann, M.; Kovac, J. *J. Chem. Phys.* **1973,** *58*, 1564. (c) Odijk, T. *Macromolecules* **1995**, *28*, 7016−7018.
(42) (a) Koutsos, V.; van der Vegte, E. W.; Pelletier, E.; Stamouli, A.; Hadziioannou, G. *Macromolecules* **1997**, *30*, 4719−4726. (b) Koutsos, V.; van der Vegte, E. W.; Grim, P. C. M.; Hadziioannou, G. *Macromolecules* **1998**, *31*, 116−123.
(43) (a) Otsu, T.; Matsunaga, T.; Kuriyama, A.; Yoshioka, N. *Eur. Polym. J.* **1989**, *25* (7/8), 643−650. (b) Otsu T.; Kuriyama, A. *Polym. Bull.* **1984**, *11*, 135−142.
(44) Cesaro, J.; Aksay, I. A.; Bleier *J. Am. Ceram. Soc.* **1988**, *71*, 250−255.
(45) (a) Inukai, I.; Mizutani, W.; Saito, K.; Shimizu, H.; Iwasawa, Y. *Jpn. J. Appl. Phys.* **1991**, *30*, 3496−3502. (b) DeRose, J. A.; Thundat, T.; Nagahara, L. A.; Lindsay, S. M. *Surf. Sci.* **1991**, *256*, 102−108. (c) Zheng, X.-Y.; Ding, Y.; Bottomley, L. A.; Allison, D. P.; Warmack, R. J. *J. Vac. Sci. Technol. B* **1995**, *13*, 1320−1324.
(46) (a) Nuzzo, R. G.; Dubois, L. H.; Allara, D. L. *J. Am. Chem. Soc.* **1990**, *112*, 558. (b) Porter, M. D.; Bright, T. B.; Allara, D. L.; Chidsey, C. E. D. *J. Am. Chem. Soc.* **1987**, *109*, 3559.
(47) de Gennes, P.-G. *Adv. Colloid. Interface Sci.* **1987**, *27*, 189−209.
(48) Sader, J. E.; Larson, I.; Mulvaney, O.; White L. E. *Rev. Sci. Instrum.* **1995**, *66* (7), 3789.
(49) (a) Bergström, L.; Bostedt, E. *Colloid Surf.* **1990**, *49*, 183−197. (b) Senden, T. J.; Drummond, C. J. *Colloid Surf.* **1995**, *94*, 29−51. (c) Tsukruk, V. V.; Bliznyuk, V. N. *Langmuir* **1998**, *14*, 446−455.
(50) (a) Guffond, M. C.; Williams, D. R. M.; Sevick, E. M. *Langmuir* **1997**, *13*, 5691−5696. (b) Jimenez, J.; Rajagopalan, R. *Eur. Phys. J. B.* **1998**, *5*, 237−243. (c) Jimenez, J.; Rajagopalan, R. *Langmuir* **1998**, *14*, 2598−2601.
(51) Israelachvili, J. *Intermolecular and Surface Forces*; Academic Press: London, 1992.
(52) Luckham, P. F.; Klein, J. *Macromolecules* **1985**, *18*, 721−728.
(53) Multiple attractive peaks were also observed in some experiments. We attribute these types of curves to single polymer chains which became adsorbed to the tip at multiple sites, i.e., the formation of adsorbed chain loops on the tip.
(54) Fleer, G. J.; Lyklema, J. In *Adsorption from Solution at the Solid−Liquid Interface*; Parfitt, G. D., Rochester, C. H., Eds.; Academic Press: New York, 1983; Chapter 4.
(55) The magnitude of bond rupture forces, F_b, and bond stiffness, k_{bond}, is predicted from the binding (dissociation) energy, E_b, using the Morse potential:[57a] $V = E_b[1 - e^{-a(r-r_{eq})}]^2$ where r_{eq} is the equilibrium bond length and a is a parameter controlling the width of the potential well. The force is then $F = -\partial V/-\partial r = 2aE_b[e^{-2a(r-r_{eq})} - e^{-a(r-r_{eq})}]$, and the bond stiffness is $k = -\partial F/\partial r = 2a^2E_b$. For C−C bonds $E_{b(C-C)} \approx 335$ kJ/mol,[57a] $r_{eq} \approx 0.154$ nm, and $a \approx 1.994 \times 10^{10}$ m^{-1}, thus giving $F_{b(C-C)} \approx 5-6$ nN and $k_{(C-C)} \approx 440$ N/m. For C−S bonds $E_{b(C-S)} \approx 325$ kJ/mol, $r_{eq} \approx 0.181$ nm, and $a \approx 1.726 \times 10^{10}$ m^{-1}, thus giving $F_{b(C-S)} \approx 4-5$ nN and $k_{(C-S)} \approx 320$ N/m. For Au−S bonds $E_{b(Au-S)} \approx 170$ kJ/mol,[57b] $r_{eq} \approx 0.242$ nm, and $a \approx 1.75 \times 10^{10}$ m^{-1}, thus giving $F_{b(Au-S)} \approx 2-3$ nN and $k_{(Au-S)} \approx 170$ N/m.
(56) (a) Drexler, K. E. *Nanosystems;* John Wiley and Sons: New York, 1992; Chapter 3. (b) Ulman, A. *Chem. Rev.* **1996**, *96*, 1533.
(57) The repulsive force on approach, $F_{approach}$, was approximated by fitting the experimental data to an empirical exponential equation of the following form: $a \exp[-x]$.
(58) We also conducted experiments as a function of strain rate (controlled by dz/dt, the z-piezo deflection rate) and found no influence over 2 orders of magnitude on the single chain entropic elasticity force profiles on retraction and subsequent calculations of a.

MA981245N